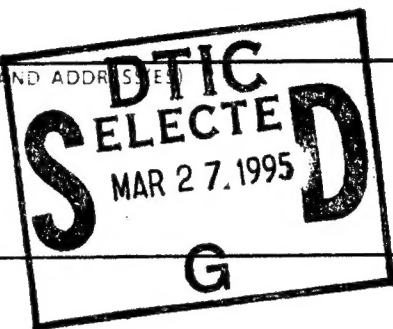


REPORT DOCUMENTATION PAGE				Form Approved OMB No 0704-0188	
<small>Public reporting burden for this collection of information is estimated to average 1 hour per response, including the time for reviewing instructions, searching existing data sources, gathering and maintaining the data needed, and completing and reviewing the collection of information. Send comments regarding this burden estimate or any other aspect of this collection of information, including suggestions for reducing this burden, to Washington Headquarters Services, Directorate for Information Operations and Reports, 1215 Jefferson Davis Highway, Suite 1204, Arlington, VA 22202-4302, and to the Office of Management and Budget, Paperwork Reduction Project (0704-0188), Washington, DC 20503.</small>					
1. AGENCY USE ONLY (Leave blank)		2. REPORT DATE		3. REPORT TYPE AND DATES COVERED FINAL	
4. TITLE AND SUBTITLE New Thin-Film Nonlinear Optical Materials: Ordered Al 1-x Inx P on GaAs				5. FUNDING NUMBERS 61102F 1602/01	
6. AUTHOR(S) Dr Vernon					
7. PERFORMING ORGANIZATION NAME(S) AND ADDRESS(ES) Spire Corporation				8. PERFORMING ORGANIZATION REPORT NUMBER AFOSR-TP 95 0145	
9. SPONSORING MONITORING AGENCY NAME(S) AND ADDRESS(ES) AFOSR/NE 110 Duncan Avenue Suite B115 Bolling AFB DC 20332-0001				10. SPONSORING MONITORING AGENCY REPORT NUMBER F49620-93-C-0055	
<div style="text-align: center;">  </div>					
11. SUPPLEMENTARY NOTES					
12a. DISTRIBUTION AVAILABILITY STATEMENT APPROVED FOR PUBLIC RELEASE: DISTRIBUTION UNLIMITED				12b. DISTRIBUTION CODE	
13. ABSTRACT (Maximum 200 words) SEE FINAL REPORT ABSTRACT					
14. SUBJECT TERMS				15. NUMBER OF PAGES	
				16. PRICE CODE	
17. SECURITY CLASSIFICATION OF REPORT UNCLASSIFIED		18. SECURITY CLASSIFICATION OF THIS PAGE UNCLASSIFIED		19. SECURITY CLASSIFICATION OF ABSTRACT UNCLASSIFIED	
				20. LIMITATION OF ABSTRACT UNCLASSIFIED	

FR-60292

Final Technical Report for
**NEW THIN-FILM
NONLINEAR OPTICAL MATERIALS:
ORDERED
 $\text{Al}_{1-x}\text{In}_x\text{P}$ ON GaAs**

Submitted under:
Contract No. F49620-93-C-0055

Submitted to:
**Air Force Office of Scientific Research
110 Duncan Avenue, Suite B115**

19950323 119



A Final Report for:
 NEW THIN-FILM NONLINEAR OPTICAL MATERIALS:
 ORDERED $\text{Al}_{1-x}\text{In}_x\text{P}$ ON GaAs

Program managed by AFOSR
 Funded by BMDO
 Contract No. F49620-93-C-0055

Contract period:
 1 August 1993 through 31 January 1994

Submitted to:
 AFOSR/PKA
 110 Duncan Avenue, Suite B115
 Bolling AFB, DC 20332-0001

Submitted by:
 Spire Corporation
 One Patriots Park
 Bedford, MA 01730-2396

Accession For	
NTIS	CRA&I <input checked="" type="checkbox"/>
DTIC	TAB <input type="checkbox"/>
Unannounced <input type="checkbox"/>	
Justification _____	
By _____	
Distribution /	
Availability Codes	
Dist	Avail and / or Special
A-1	

WARNING: This document contains technical data whose export is restricted by the Arms Export Control Act (Title 22, U.S.C., Sec 2751, et seq.) or the Export Administration Act of 1979, as amended, Title 50, U.S.C., App. 2401, et seq. Violations of these export laws are subject to severe criminal penalties. Disseminate in accordance with the provisions of AFR 80-34.

TABLE OF CONTENTS

	<u>Page</u>
1 EXECUTIVE SUMMARY	1
2 BACKGROUND	1
2.1 Growth of Ordered $\text{Al}_{1-x}\text{In}_x\text{P}$	1
2.2 Nonlinear Optical Properties of $\text{Al}_{1-x}\text{In}_x\text{P}$ on GaAs	2
3 EXPERIMENTAL	3
3.1 Film Growth	3
3.2 Characterization	6
3.3 Non-destructive Measurement of AlInP Layer Thickness	8
3.4 Results	9
3.5 Measurement of Birefringence at Wright Laboratories	10
3.6 Low-temperature Photoluminescence Measured at The National Renewable Energy Laboratories (NREL) by Dr. R. Ahrenkiel	10
3.7 Low-temperature Photoluminescence Measured at The University of Utah (Dr. M. Delong)	11
3.8 Transmission Electron Microscopy Performed at NREL by Dr. Kim M. Jones	12
4 CONCLUSIONS	12
5 PHASE II IDEAS	13
6 REFERENCES	15

LIST OF ILLUSTRATIONS

		<u>Page</u>
1	Atomic ordering along (111)-type directions in the structure of $\text{Ga}_{1-x}\text{In}_x\text{P}$ on GaAs	1
2	Photoluminescence wavelength at room temperature versus tilt angle of $\text{Ga}_{0.51}\text{In}_{0.49}\text{P}$ grown by MOCVD on GaAs wafers of near-(100) orientations	3
3	SPI-MOCVD™ 450 schematic	4
4	Structure studied in Phase I experiments	5
5	Representation of the various tilt directions for the vicinal (100) GaAs substrates of Phase I	5
6	Sample X-ray rocking curve data for run MO5-2754; lattice mismatch = 872 ppm, $\text{Al}_{1-x}\text{In}_x\text{P}$ full width half maximum = 39 arcsec	7
7	Film thickness measurement by optical-reflectance spectroscopy modelling of $\text{Al}_{1-x}\text{In}_x\text{P}$ on GaAs (sample MO5-2889-2)	7
8	Film thickness measurement by optical-reflectance spectroscopy modelling of $\text{Al}_{1-x}\text{In}_x\text{P}$ on GaAs (sample MO5-2739)	8
9	$\text{Al}_{1-x}\text{In}_x\text{P}$ and $\text{Al}_x\text{Ga}_{1-x}\text{As}$ bandgaps versus Al fraction	9
10	Spectroscopic ellipsometry data for sample MO5-2762-2, $\text{Al}_{1-x}\text{In}_x\text{P}$ grown on GaAs tilted towards (111)B	10
11	5K photoluminescence from sample MO-2889-1, measured at NREL	11
12	Comparison of 5K PL spectra from the four $\text{Al}_{1-x}\text{In}_x\text{P}$ samples analyzed at the University of Utah	12
13	Electron diffraction pattern of sample MO5-2889-1 on the [031] zone pass measured at NREL	13
14	Basic design of the high-power visible laser to be developed; facet passivation uses an overgrown layer of disordered $\text{Ga}_{0.51}\text{In}_{0.49}\text{P}$ on etched laser facets	14

LIST OF TABLES

	<u>Page</u>
I Growth parameters for the experiments of Phase I	4
II Description of samples grown in Phase I	6

1 EXECUTIVE SUMMARY

The basic goal of this program is to identify growth parameters which lead to the most ordering, and most birefringence, in $\text{Al}_{1-x}\text{In}_x\text{P}$ lattice-matched to GaAs. Birefringence is necessary for the practical use of $\text{Al}_{1-x}\text{In}_x\text{P}$ as a non-linear optical material. Epitaxial growth is by metalorganic chemical vapor deposition (MOCVD). The major characterization tools include double-crystal X-ray rocking curve analysis to determine composition, low-temperature photoluminescence (PL) to determine bandgap, and transmission electron diffraction to determine ordering.

2 BACKGROUND

2.1 Growth of Ordered $\text{Al}_{1-x}\text{In}_x\text{P}$

Study of $\text{Al}_{1-x}\text{In}_x\text{P}$ very often involves the question of atomic ordering,¹⁻¹⁶ since bandgap can vary as much as 0.1 eV with the degree of ordering. Although most III-V alloys can show some ordering behavior,⁹ $\text{Al}_y\text{Ga}_{1-x-y}\text{In}_x\text{P}$, of which $\text{Al}_{1-x}\text{In}_x\text{P}$ is a subset where $x+y = 1$, is known to show the strongest effects.¹ Ordering is of the CuPt type, with (Al)Ga- and In-sublattices ordering along (111)-type axes, as shown in Figure 1; actual directions of ordering are reported to be the (-1,1,1) and (1,-1,1) variants.⁴ Ordered material is composed of "domains" where atomic sublattice ordering is present, separated by regions of disordered material. These ordered domains may be 10 to 50 nm in size. Highly ordered material may have more than 50% of its volume in these ordered domains, while "disordered" material has less than 1% in them.

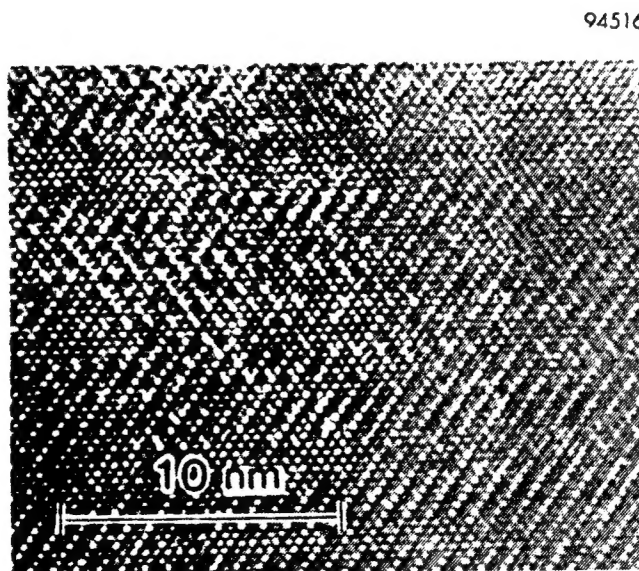


Figure 1 Atomic ordering along (111)-type directions in the structure of $\text{Ga}_{1-x}\text{In}_x\text{P}$ on GaAs.

Ordering in $\text{Al}_y\text{Ga}_{1-x-y}\text{In}_x\text{P}$ is strongly dependent on the growth method: MOCVD shows strongest ordering, chloride-CVD shows weak ordering, and liquid-phase epitaxy (LPE) shows no ordering at all.¹ Differences may be related to growth temperatures and rates involved in these methods. Ordering in MOCVD-grown $\text{Al}_y\text{Ga}_{1-x-y}\text{In}_x\text{P}$ seems independent of growth pressure, but has been reported to be a complex function of growth temperature and rate.¹⁵ This is because the ordering observed is a function of both surface adatom kinetics and bulk atomic interdiffusion phenomena,¹⁵ which often have very different dependencies upon growth temperature and rate.

Furthermore, there are typically effects due to both short- and long-range ordering and to uniformity of ordering. Because "degree of ordering" depends on which parameter is being used as the criterion and on the measurement techniques employed, published results are difficult to interpret. Thus, growth conditions which yield the "most" ordering are not easily obtainable from the literature. For instance, Okuda *et al.*,¹⁰ report that the size of ordered domains in a $\text{Ga}_{1-x}\text{In}_x\text{P}$ layer is maximum at a growth temperature of $\sim 650^\circ\text{C}$, but that the total amount of ordered material is maximum at $\sim 590^\circ\text{C}$.

Degree of order in an $\text{Al}_y\text{Ga}_{1-x-y}\text{In}_x\text{P}$ layer grown by MOCVD depends not only on growth temperature and rate, but also on substrate orientation and film doping. Ordering is present only in films grown on (100) or near-(100) surfaces,⁴ but ordering versus tilt angle is dependent on the direction of the tilt, as shown in Figure 2.¹⁷ In this figure, the longest wavelength (smallest bandgap) represents the most ordered film. For (100) substrates tilted towards [111]A, the amount of ordering decreases monotonically with angle. However, for wafers tilted towards [111]B, ordering rises from 0° to 5° , at which point it again decreases. For tilt angle $\geq \approx 15^\circ$, material is always disordered, independent of growth conditions.⁸ Dependence of ordering in $\text{Al}_y\text{Ga}_{1-x-y}\text{In}_x\text{P}$ is nearly identical to that shown here for $\text{Ga}_{1-x}\text{In}_x\text{P}$. Variation with tilt angle is strong evidence that surface steps play a dominant role in the ordering phenomenon. For any dopant species, a level above 10^{18} cm^{-3} causes $\text{Al}_y\text{Ga}_{1-x-y}\text{In}_x\text{P}$ to become disordered;⁴ also, high selenium concentrations have been shown to improve surface morphology.²

As explained in Kurtz *et al.*,¹⁵ effects of growth temperature and rate are very complicated. While smooth, single-crystal $\text{Ga}_{1-x}\text{In}_x\text{P}$ can be grown over the range 550 to 730°C ,¹⁷ temperature regimes reported to give the most ordering are about 625°C or 675°C , depending on other conditions.⁴ Typically, slow growth favors ordering,¹⁴ but fast growth causes increased ordering under some conditions. V-III ratio may also have an effect. For atmospheric pressure growth, the typical V-III ratio is 60 to 160, and at reduced reactor pressures, ratios of 100 to 400 are often used; higher PH_3 flows are needed to compensate for decreased pyrolysis, due to decreased residence time, at lower pressures. At higher growth temperatures, higher V-III ratios lead to increased ordering, while at lower temperatures, the opposite is observed.⁴

2.2 Nonlinear Optical Properties of $\text{Al}_y\text{In}_x\text{P}$ on GaAs

The material system designated as $(\text{Al}_x\text{Ga}_{1-x})_{0.5}\text{In}_{0.5}\text{P}$, lattice-matched to GaAs, has the following attributes:

- Ordered III-V materials are non-centrosymmetric and show large second-order nonlinear optical susceptibility

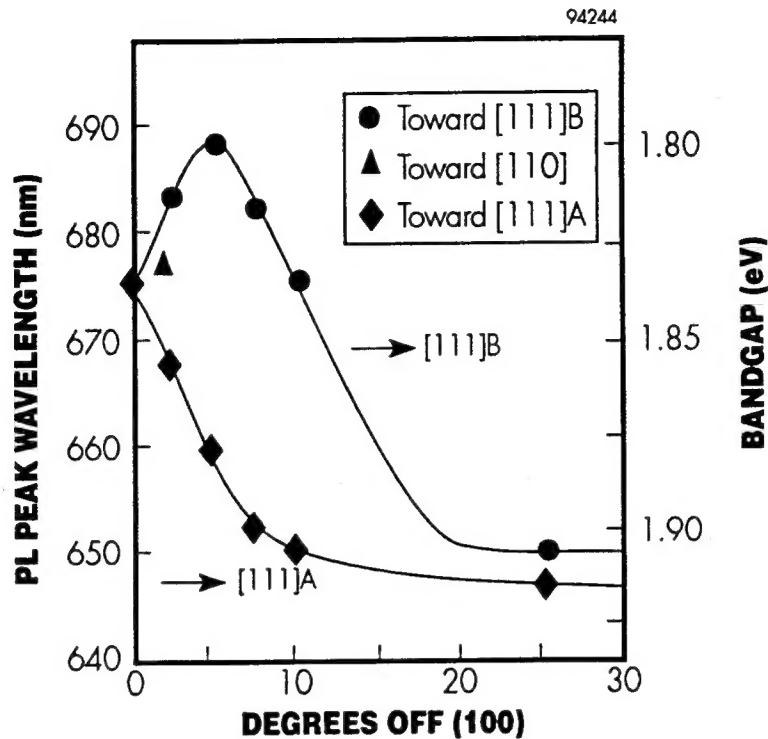


Figure 2 Photoluminescence wavelength at room temperature versus tilt angle of $Ga_{0.51}In_{0.49}P$ grown by MOCVD on GaAs wafers of near-(100) orientations. (From reference 17.)

- $(Al_xGa_{1-x})_{0.5}In_{0.5}P$ shows the most group-III ordering of any III-V material system
- $Ga_{0.51}In_{0.49}P$ has a large χ^2 value, $\approx 100 \times 10^{-12}$ m/V; $Al_{1-x}In_xP$ is expected to be similar
- $Al_{0.51}In_{0.49}P$ is transparent for: ≥ 530 nm; bandgap is indirect at ≈ 2.33 eV
- $Al_{1-x}In_xP$ can be exactly lattice-matched to GaAs (when $x = 0.49$)
- Ordering on {111} implies that the optical axis is tilted 55° from the surface; this implies the wavelength is tunable by rotation when used in an optical parametric oscillator.

3 EXPERIMENTAL

3.1 Film Growth

All films in this work were grown by low-pressure MOCVD, in the SPI-MOCVD™ 450 reactor. Figure 3 is a schematic representation of the growth system.

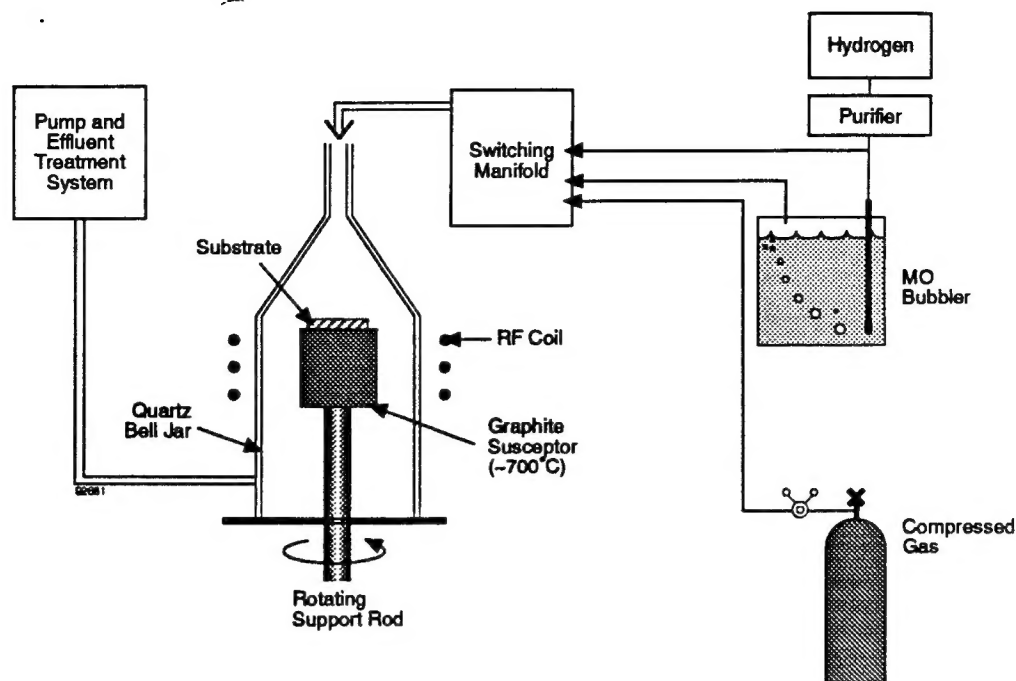


Figure 3 SPI-MOCVD™ 450 schematic.

The parameters varied in Phase I include growth temperature, V-III ratio, growth rate, and substrate tilt direction. All films were grown without intentional dopants; conditions used are listed in Table I. The structure studied is pictured in Figure 4. Substrate tilt directions are shown diagrammatically in Figure 5.

Table I Growth parameters for the experiments of Phase I.

Parameter	Value
Reactor	SPI-MOCVD™ 450
Pressure	76 torr
Reagents	trimethylindium (TMI) at 20°C trimethylaluminum (TMA) at 17°C arsine (AsH ₃) 100% phosphine (PH ₃) 100%
GaAs Substrates	(100), 3° towards [111]A, [111]B, [110], and [10 $\bar{1}$]
Al _(1-x) In _(x) P thickness	≈1-2 μm
Growth temperature	625-725°C
Growth rate	1-3 Å/sec
V - III ratio	≈100-2000

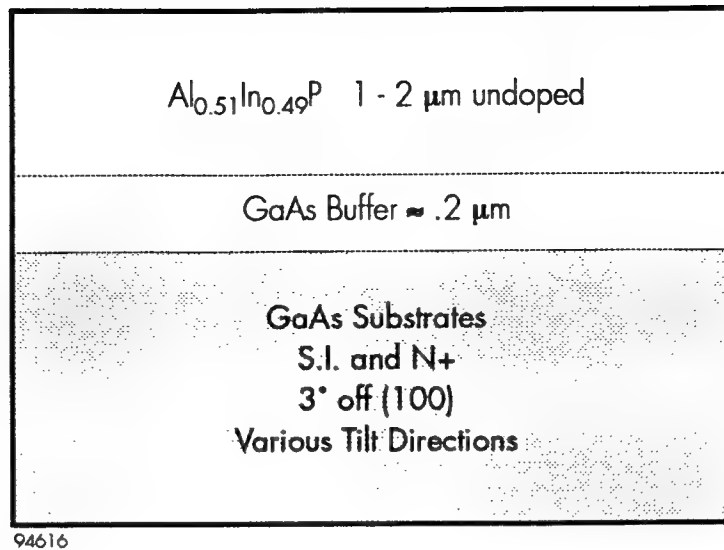


Figure 4 Structure studied in Phase I experiments.

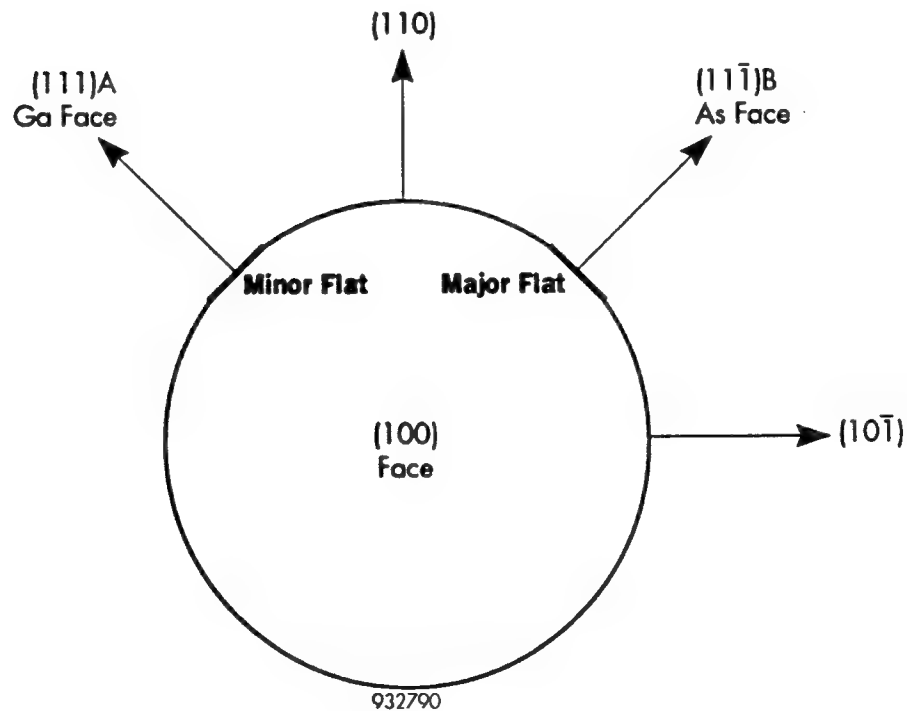


Figure 5 Representation of the various tilt directions for the vicinal (100) GaAs substrates of Phase I.

The experimental procedure was to calibrate the TMA flow for lattice-matched $\text{Al}_{1-x}\text{In}_x\text{P}$ at each set of growth conditions; TMI flow was varied intentionally to explore different growth

rates. The lattice-matching target for each test run was 1000 ppm or better [mismatch defined as (substrate lattice - film lattice)/substrate lattice]. After calibration of lattice-matching, four substrate types were loaded for growth of the test run.

Films of $\text{Al}_{(1-x)}\text{In}_{(x)}\text{P}$, $x \approx 0.49$ were grown on GaAs under many different growth conditions. In each growth run, four substrates tilted 3° toward different crystal directions were used. These directions are shown in Figure 5; the growth conditions explored are shown in Table II.

Table II *Description of samples grown in Phase I.*

Run Number	Temperature (°C)	Growth rate (Å/sec)	V - III ratio
2743	725	2.6	370
2750	625	2.3	137
2762	725	2.2	137
2882	675	1.0	1801
2886	725	1.0	1847
2889	700	1.0	1888
2890	625	1.1	1825

Lattice-matching to within ≈ 1000 ppm was calibrated at each set of growth conditions using double-crystal X-ray rocking curve analysis to measure composition. At each condition, a mirror-like surface morphology was obtained.

3.2 Characterization

Composition (mismatch) was determined by double-crystal X-ray rocking curve analysis; sample X-ray data is shown in Figure 6. Surface quality was checked by Nomarski interference-contrast microscopy; lattice-matched films have smooth, specular surfaces. Film thickness was determined by optical-reflectance spectroscopy.¹⁸ A sample measurement is shown in Figure 7; the short-wavelength data above the bandgap energy is not relevant here; thickness is obtained by fitting the data at wavelengths longer than ≈ 530 nm.

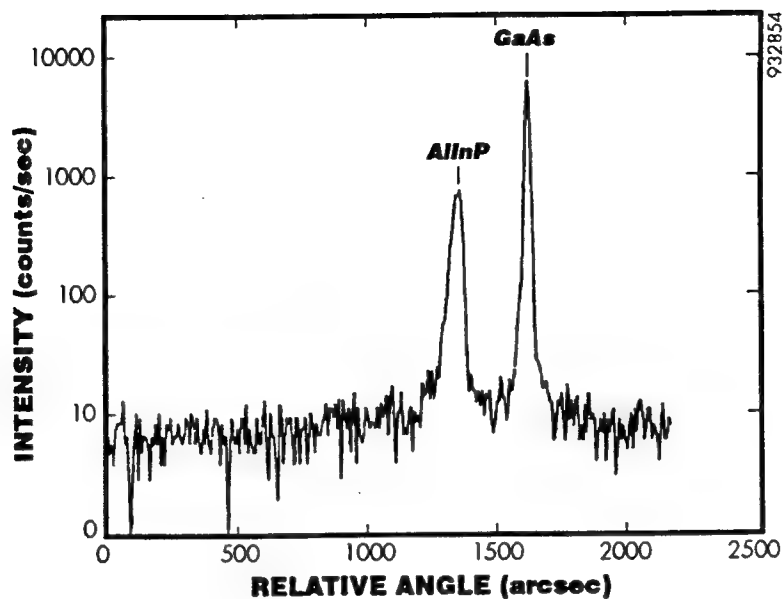


Figure 6 Sample X-ray rocking curve data for run MO5-2754; lattice mismatch = 872 ppm, $Al_{1-x}In_xP$ full width half maximum = 39 arcsec.

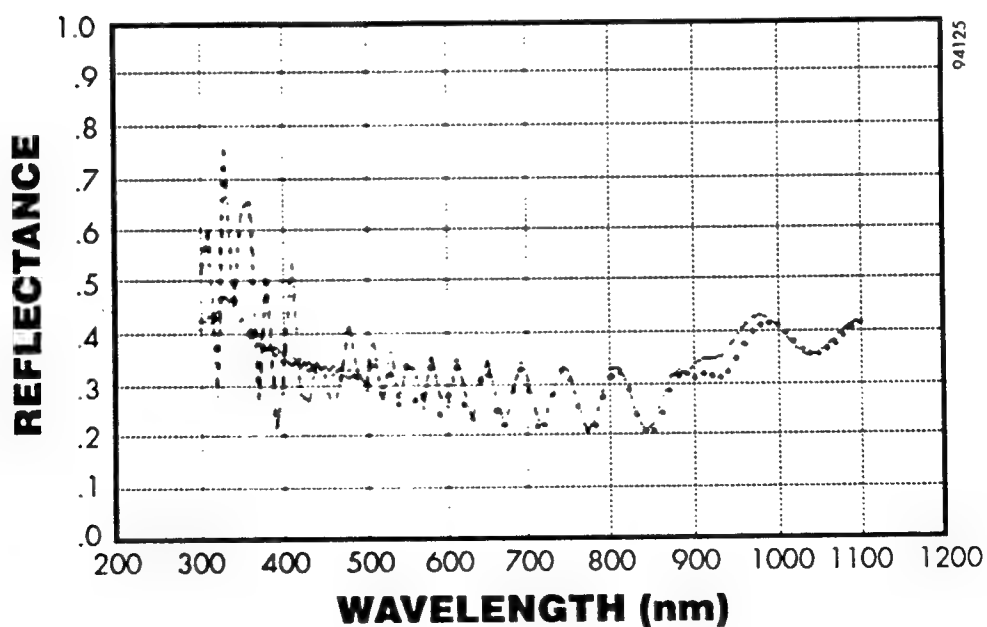


Figure 7 Film thickness measurement by optical-reflectance spectroscopy modelling of $Al_{1-x}In_xP$ on GaAs (sample MO5-2889-2). Measured thickness is 1.29 μm .

3.3 Non-destructive Measurement of AlInP Layer Thickness

The thickness of nearly-lattice-matched AlInP layers on GaAs substrates was measured non-destructively using optical reflectance spectroscopy (ORS).¹⁸ In ORS, a near-normal-incidence specular reflectance spectrum is collected, and thickness and composition of the layer are determined by a least-squares fit of a thin film optical model of the data. REFIT, a computer program developed for the analysis of AlGaAs/GaAs structures by ORS, was used to perform the least-squares fits.

Good fits (Figure 8) were obtained by substituting the optical properties of high-aluminum composition ($x \approx 0.8$) AlGaAs for those of lattice-matched AlInP ($x \approx 0.5$) in the reflectance calculations. The fact that this works is not too surprising when the variation in band gap energy for AlInP and AlGaAs are compared. Figure 9 shows both the direct (Γ) and indirect (X) band gap energies of both AlInP and AlGaAs as a function of composition. The direct band gap energy, E_{Γ} , is a strong function of composition in both AlInP and AlGaAs. The value of E_{Γ} for AlInP is essentially the same as that of AlGaAs after shifting the curve by about 0.25 in composition. Since, in both materials, E_X is nearly independent of composition, any composition-dependent optical properties must derive from the direct band features.

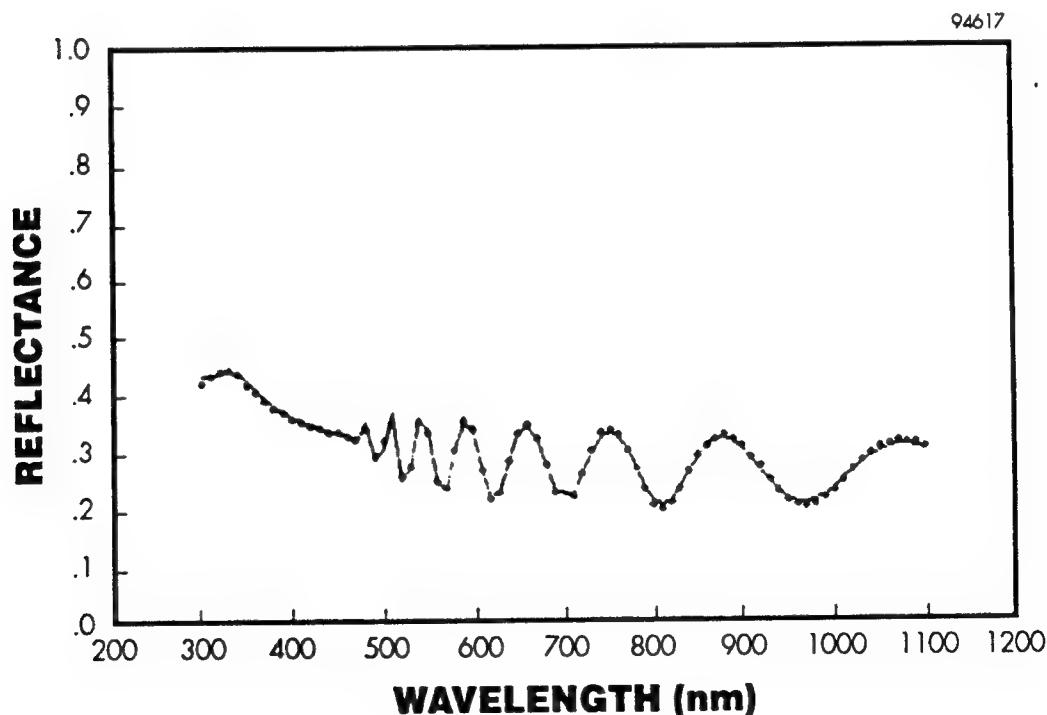


Figure 8 *Film thickness measurement by optical-reflectance spectroscopy modelling of $Al_{1-x}In_xP$ on GaAs (sample MO5-2739). Measured thickness is 0.71 μm .*

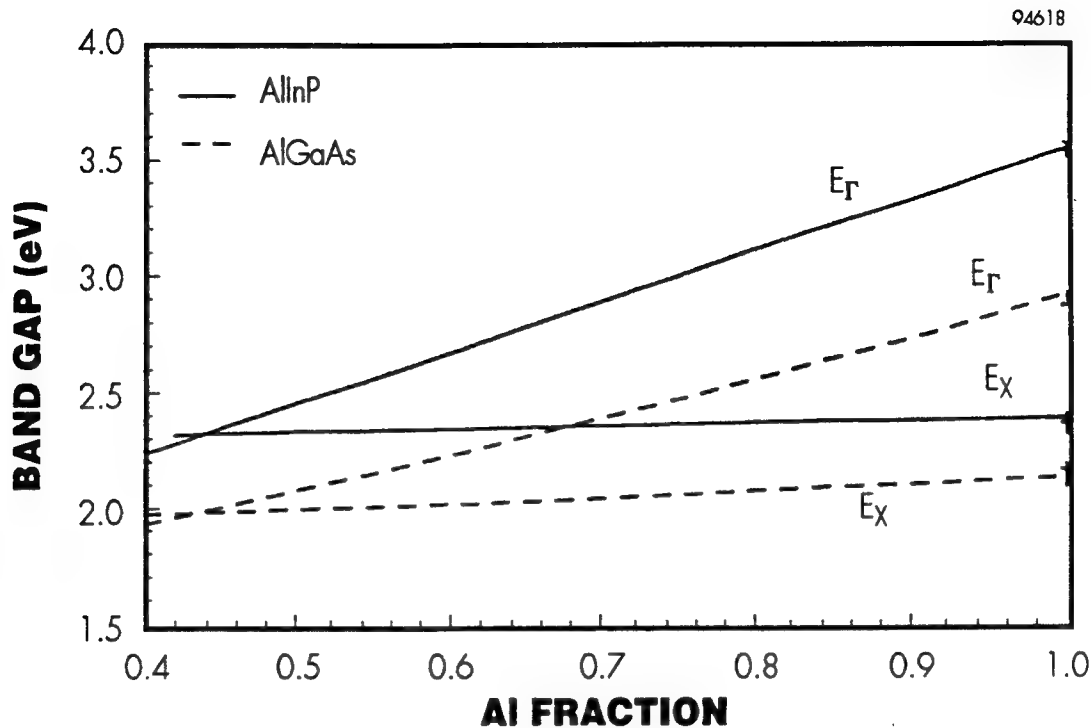


Figure 9 $Al_{1-x}In_xP$ and $Al_xGa_{1-x}As$ bandgaps versus Al fraction.

3.4 Results

High-resolution X-ray diffraction (HRXRD) was used in an attempt to observe ordering in $Ga_{0.51}In_{0.49}P$ layers. $Ga_{1-x}In_xP$ was used instead of $Al_{1-x}In_xP$ since ordered films could be easily identified by photoluminescence data. The method of Liu *et al.*,¹⁹ was used to search for reflections from GaP/InP superlattice planes.

Measurements were performed with a Blake Instruments diffractometer equipped with a four-crystal Ge monochromator using $CuK\alpha_1$ radiation. Data was recorded with a scintillation counter and all measurements were made with ω and 2θ uncoupled. Asymmetric {115} reflections were used in a search for the ordered structure on the column-III sublattice. The ordered structure behaves like a GaP/InP superlattice in [115] directions with the period

$$D = d_{InP} + d_{GaP} \approx 2d_{GaAs}. \quad (1)$$

The Bragg angle (θ) corresponding to this superlattice is 20.733° , and the incident angle ω is 4.94° .

Measurements were performed on a number of samples grown under a variety of conditions, but no diffraction peaks associated with GaInP ordering were detected. The sensitivity of the method with this equipment is unknown and it remains unclear whether or not this negative result indicates a lack of GaInP ordering.

3.5 Measurement of Birefringence at Wright Laboratories

Samples of $\text{Al}_{1-x}\text{In}_x\text{P}$ were evaluated for birefringence through the courtesy of Dr. Mel Ohmer at Wright Laboratory; measurement consists of spectroscopic ellipsometry to determine refractive index versus angle and wavelength. Typical data are shown in Figure 10; birefringence would show up as a variation in refractive index versus azimuth. By looking at the ridge of the surface plot, it can be easily seen that index versus azimuthal direction (into the page) appears to vary; this indicates birefringence in the sample.

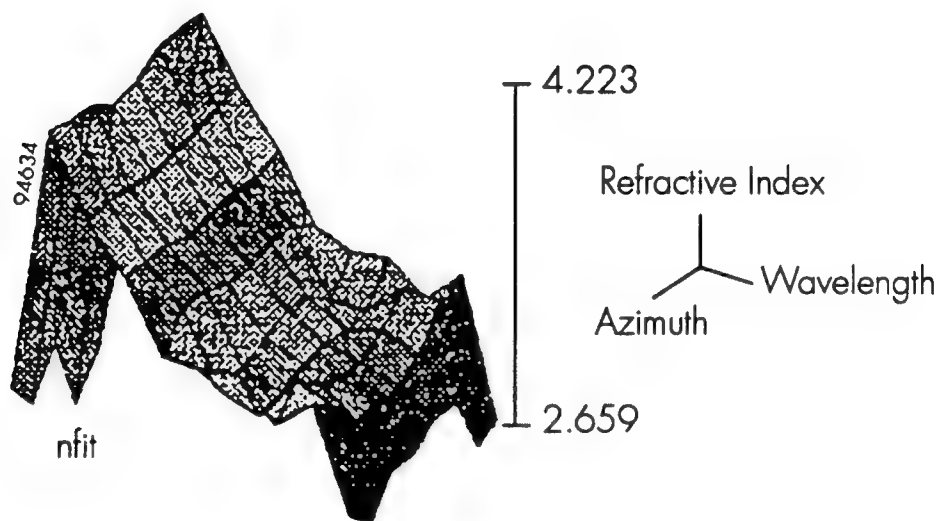


Figure 10 *Spectroscopic ellipsometry data for sample MO5-2762-2, $\text{Al}_{1-x}\text{In}_x\text{P}$ grown on GaAs tilted towards (111)B. Data from Dr. Mel Ohmer, Wright Laboratories.*

A possible explanation for the fact that birefringence does not appear more strongly is as follows: In PL measurements, the ordered domains will have a disproportionately large effect on the signal, due to carrier migration into small-bandgap regions. Although we believe (from symmetry considerations) that an ordered domain would show strong birefringence, the variation in the orientation of the individual domains leads to an averaging process in the ellipsometry measurement.

3.6 Low-temperature Photoluminescence Measured at The National Renewable Energy Laboratories (NREL) by Dr. R. Ahrenkiel

Photoluminescence at 5K was observed from samples MO5-2889-1, grown on a substrate with a (111)B tilt, and MO5-2889-2, grown on the (111)A tilt. PL data from MO-2889-1 is shown in Figure 11. Comparing these two samples shows that the bandgap, assumed to be indicated by the highest-intensity peak, shifts by 70 MeV, with the B sample being the lower energy. This may reveal that the B sample is more ordered than the A sample. This result is quite analogous to what we have found in our study of $\text{Ga}_{1-x}\text{In}_x\text{P}$, where (111)B-tilted samples were found to be more ordered (lower bandgap) than the ones grown on (111)A, with an energy difference as great as 100 MeV.

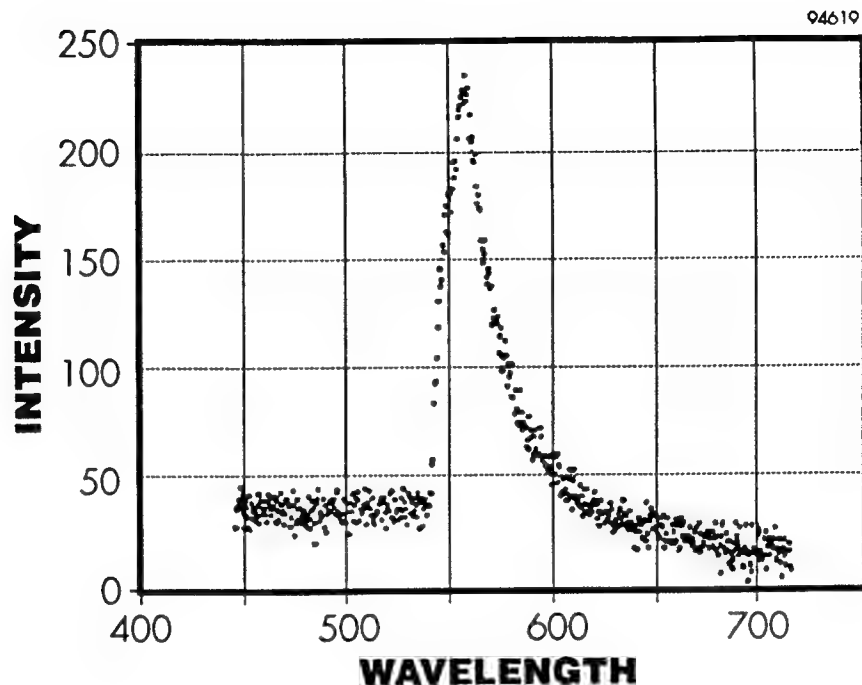


Figure 11 5K photoluminescence from sample MO-2889-1, measured at NREL.

3.7 Low-temperature Photoluminescence Measured at The University of Utah (Dr. M. Delong)

Figure 12 shows 5K photoluminescence data on four samples. The dominant peak for sample 2762 shows very little shift (8 MeV) as we compare the number 1 and 2 samples [grown on (111)A and (111)B]. However there is a large energy shift (82 MeV, comparing the two orientations) for the 2882 samples. This would indicate strong ordering in run 2882, but not in 2762. This seems to make sense, looking at the growth parameters. However, the bandgap differences are in the opposite direction from those found in our study of $\text{Ga}_{1-x}\text{In}_x\text{P}$. In the $\text{Al}_{1-x}\text{In}_x\text{P}$ data, the "B" samples have higher energy than the "A" ones. It may be that the effects of tilt direction are not the same as in the better-understood $\text{Ga}_{1-x}\text{In}_x\text{P}$ system.

For run 2862, growth temperature was 725°C, rate was 2.2Å/sec, and the V-III ratio was 137. For 2882, growth temperature was 675°C, rate was 1.0Å/sec, and V-III ratio was 1801. In our recent $\text{Ga}_{1-x}\text{In}_x\text{P}$ study we clearly identified growth conditions which lead to order, or disorder, and it appears the same trends apply here. Ordering is most favored by a growth temperature $\approx 675^\circ\text{C}$, a low growth rate, and a high V-III ratio. These are all parameters which would lead to reduced surface mobility. On the other hand, increased surface mobility conditions (higher temperature, lower V-III) lead to greater disorder.

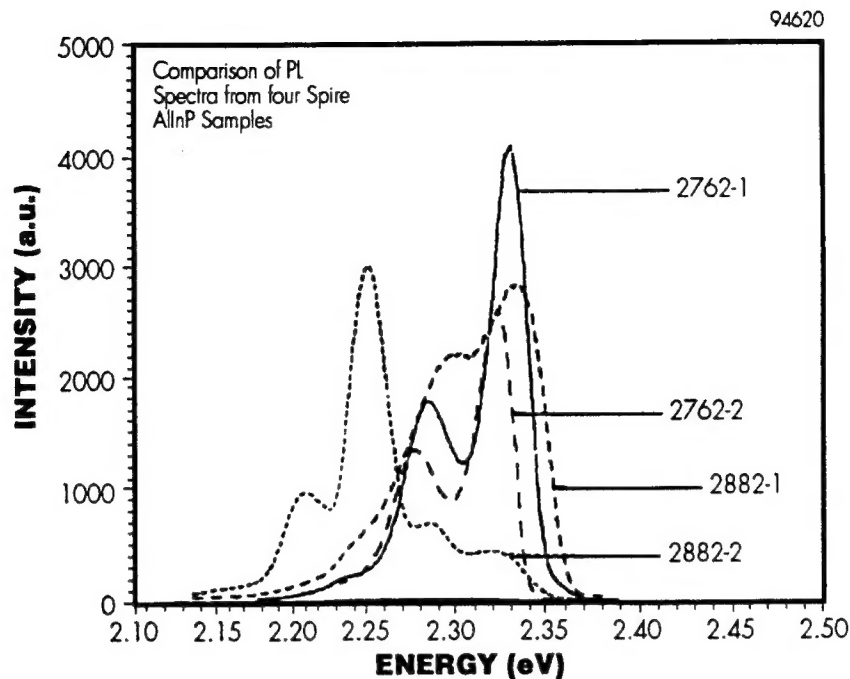


Figure 12 Comparison of 5K PL spectra from the four $Al_{1-x}In_xP$ samples analyzed at The University of Utah.

3.8 Transmission Electron Microscopy Performed at NREL by Dr. Kim M. Jones

Samples MO5-2889-1 and MO5-2889-2 were sent to NREL for examination by transmission electron microscopy. These samples had been grown at 700°C on (100) substrates misoriented 3° toward the (111)B and (111)B directions, respectively. Electron diffraction patterns were taken on the [031] type zone axis to identify ordering. Both of the samples have $\frac{1}{2}(113)$ spots, which is evidence of CuPt type ordering on the (111). Figure 13 shows a photograph of the diffraction pattern of sample MO5-2889-1 (grown on a (100)⇒(111)B substrate); the smaller spots labeled $\frac{1}{2}(113)$ are evidence of CuPt type ordering. Electron microprobe measurements of the composition were consistent with the $Al_{50.6}In_{49.4}P$ composition derived from X-ray rocking curves.

4 CONCLUSIONS

From the experiments of Phase I, the following conclusions may be drawn:

- MOCVD produces high-quality $Al_{1-x}In_xP$ with excellent uniformity and repeatability
- By proper choice of growth conditions, MOCVD can produce ordered films, as determined by electron diffraction.

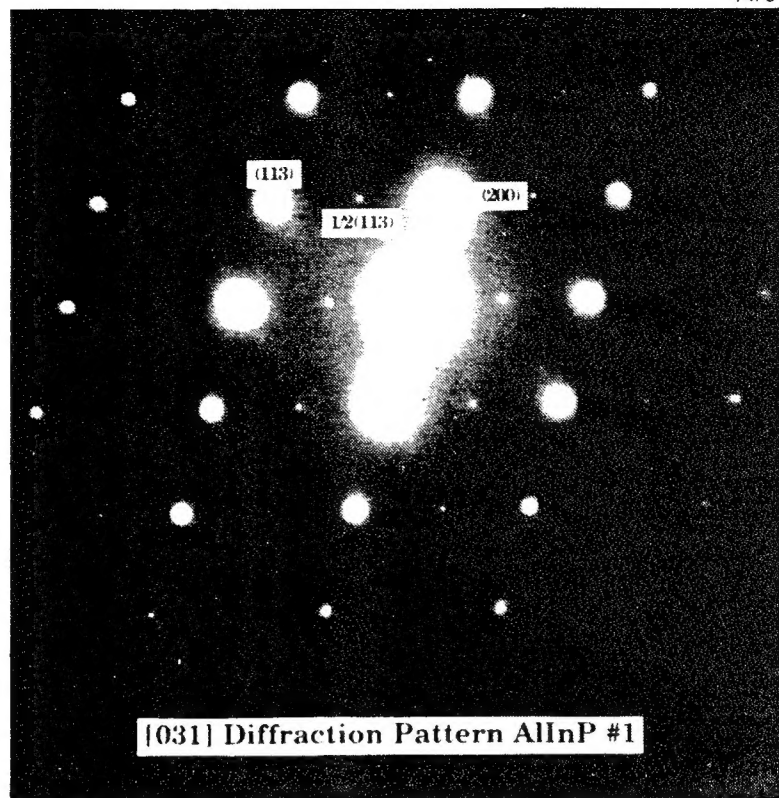


Figure 13 *Electron diffraction pattern of sample MO5-2889-1 on the [031] zone pass measured at NREL.*

- Spectral ellipsometry data taken at Wright Laboratories show weak birefringence (variation in refractive index versus azimuthal angle on the wafer) in our ordered $\text{Al}_{1-x}\text{In}_x\text{P}$ films
- Using conditions which favor highly ordered growth, the bandgap among the two substrate types studied varies as much as 82 MeV; for conditions which give disordered growth, the same bandgap variation is only 8 MeV
- The most disordering is observed at $\approx 725^\circ\text{C}$ growth temperature, and a low V-III ratio (≈ 100)
- The most ordering is observed at $\approx 675^\circ\text{C}$, high V-III ratio (≈ 1800).

5 PHASE II IDEAS

Phase II will seek to demonstrate that growth of highly ordered $\text{Al}_y\text{Ga}_{1-x-y}\text{In}_x\text{P}$ can be used to solve a serious problem in a present-day, commercially- important product. The basic objective is to use disordered $\text{Ga}_{0.51}\text{In}_{0.49}\text{P}$ as a non-absorbing facet-passivation layer to improve reliability of high-power visible diode lasers, thus greatly reducing catastrophic optical mirror damage (COMD). The active quantum well will be lower bandgap, ordered $\text{Ga}_{1-x}\text{In}_x\text{P}$. Phase II will also develop a facet-etching scheme for wafer-scale processing of lasers, thereby increasing

fabrication yields while significantly reducing production costs. Facet etching allows the growth of $\text{Ga}_{1-x}\text{In}_x\text{P}$ facet-passivation layers to be done at the wafer level, thereby avoiding the problem of handling, and possibly degrading, the delicate facets of individual laser bars.

The basic diode laser proposed is shown in Figure 14. All layers would be grown by MOCVD, with $\text{Al}_x\text{Ga}_{1-x}\text{As}$ clad layers for increased thermal- and electrical conductivity. The disordered $\text{Ga}_{1-x}\text{In}_x\text{P}$ transparent passivation layers will greatly reduce the power dissipation/heating problem at the facet mirrors, thus greatly reducing facet damage and increasing maximum-operating power and reliability.

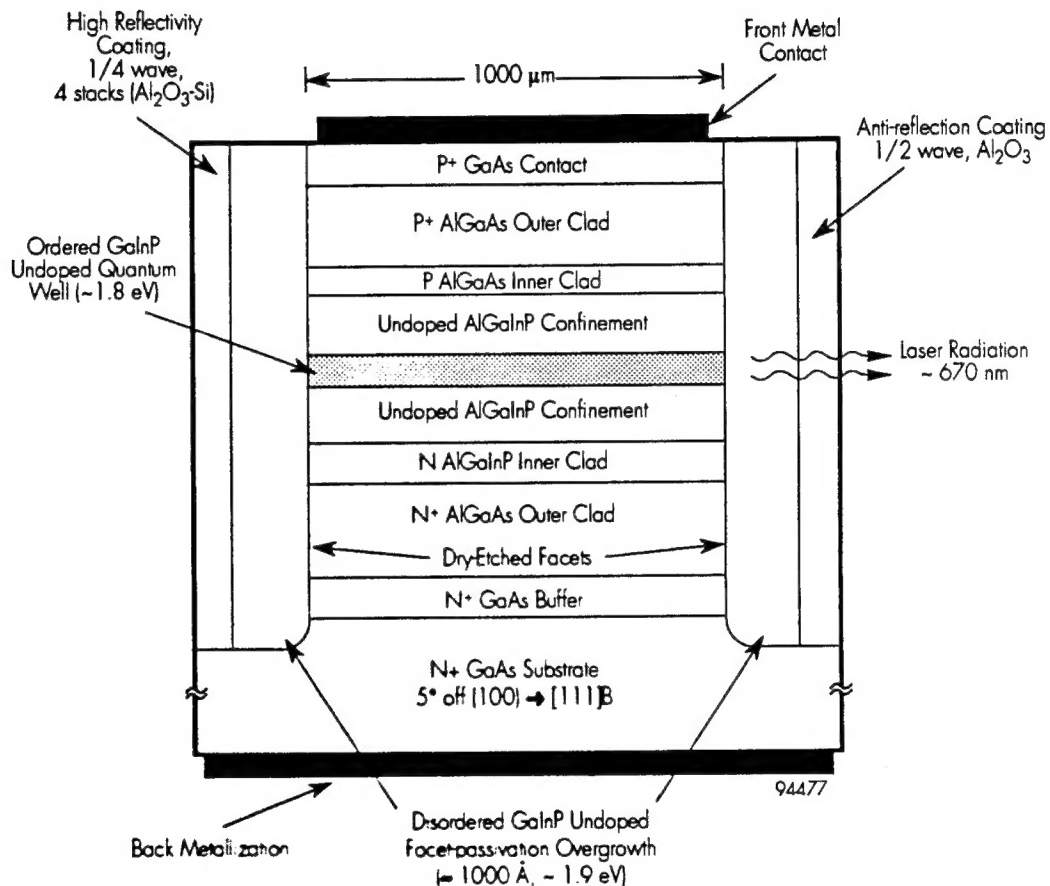


Figure 14 Basic design of the high-power visible laser to be developed; facet passivation uses an overgrown layer of disordered $\text{Ga}_{0.51}\text{In}_{0.49}\text{P}$ on etched laser facets.

Phase II will grow, fabricate, and characterize visible lasers. The ordered $\text{Ga}_{1-x}\text{In}_x\text{P}$ quantum-well material, $\approx 100\text{\AA}$ thick, has a bandgap of $\approx 1.8\text{ eV}$ (implies 689 nm). Exact lasing wavelength is determined by quantum confinement, In composition, and strain. The resulting wavelength for our preliminary design will be $\approx 670\text{ nm}$. Disordered $\text{Ga}_{1-x}\text{In}_x\text{P}$ facet passivation is transparent at wavelengths above 653 nm (1.9 eV), and thus will be a non-absorbing coating. The use of compressive strain in the quantum well leads to lower threshold current without degrading device reliability.

For a manufacturable facet-passivation process, diode lasers will be fabricated in whole-wafer form, with cleaving into individual bars only as the final step. Wafer-scale processing will lead to improved yields and lower production costs. Facets will be formed by dry etching, which has received limited use for visible lasers, but is a process demonstrated for GaAs-Al_xGa_{1-x}As and InP-Ga_{1-x}In_xAs_{1-y}P_y. By its inherent planarizing tendency, MOCVD growth of the Ga_{1-x}In_xP passivation layer will smooth any slight roughness left by the dry-etching process. There will be no significant reflection at the etched-facet-to-passivation interface, due to index matching. Lack of aluminum at the facet means reliable, non-oxidizing mirrors.

Wavelength adjustment would be accomplished by choosing the correct In composition and quantum-well thickness. Many wavelengths in the visible range are important, depending on the application. Photodynamic therapy (PDT) uses several different wavelengths between 650 and 700 nm, depending on the particular dye to be activated. For example, benzoporphyrine derivative monoacid (BPD) is best activated at ≈690 nm; other common dyes need 664 and 675 nm lasers. Chromium-doped alexandrite lasers are efficiently pumped at 680.4 nm and LiCaAlF₆ (LiCAF) and LiSrAlF₆ (LiSAF) solid-state lasers have broad absorption bands in this spectral region, making them ideal candidate for use with 600 to 700 nm diode laser pumps. Data communications through polymer optical fibers work well at 670 nm. Success in the proposed technology will lead to rapid commercialization by inclusion of visible lasers into Spire's product line of diode lasers operating near 800 nm, and 2000 nm (under development).

6 REFERENCES

1. O. Ueda, *et al.*, *J. Appl. Phys.* **68**, 8, (1990).
2. S.R. Kurtz, *et al.*, *Journal of Electronic Materials*, **19**, 8, (1990).
3. M. Kondow, *et al.*, *Appl Phys. Lett.*, **53**, 21, (1988).
4. S.R. Kurtz, *et al.*, *AIP Conf. Proceedings* 268, Denver, CO (1992).
5. H. Okuda, *et al.*, *Appl. Phys. Lett.*, **55**, 21, (1989).
6. T. Katsuyama, *et al.*, *Sumitomo Electric Technical Review* **30**, (1990).
7. K. Meehan, *et al.*, *Appl. Phys. Lett.*, **54**, 21, (1989).
8. T.Y. Wang, *et al.*, *Appl. Phys. Lett.*, **60**, 8, (1992).
9. O. Ueda, *et al.*, *Appl. Phys. Lett.*, **54**, 23, (1989).
10. H. Okuda, *et al.*, *Appl. Phys. Lett.*, **55**, 7, (1989).
11. F.P. Dabkowski, *et al.*, *Appl. Phys. Lett.*, **52**, 25, (1988).
12. P. Bellon, *et al.*, *Appl. Phys. Lett.*, **52**, 7, (1988).
13. M.K. Lee, *et al.*, *Appl. Phys. Lett.*, **59**, 25, (1991).
14. D.S. Cao, *et al.*, *J. Appl. Phys.* **66**, 11, (1989).
15. S.R. Kurtz, *et al.*, *Appl. Phys. Lett.*, **57**, 18, (1990).
16. H. Okuda, *et al.*, *Appl. Phys. Lett.*, **55**, 21, (1989).
17. N. Buchan, W. Heuberger, A. Jakubowicz, and P. Roentgen, *Inst. Phys. Conf.* **120**, 529, (1991).
18. M.M. Sanfacon and S.P. Tobin, *IEEE Trans. Electr. Dev.* **37**, 450 (1991).
19. Q. Liu, H. Lakner, F. Scheffer, A. Lindner, and W. Prost, *J. Appl., Phys.* **73**, 2770 (1993).